Hindawi
International Journal of Photoenergy
Volume 2020, Article ID 8740825, 9 pages
https://doi.org/10.1155/2020/8740825

Research Article

Study of the Effect of TiO_2 Layer on the Adsorption and Photocatalytic Activity of TiO_2-MoS_2 Heterostructures under Visible-Infrared Light

N. Cruz-González,[1] O. Calzadilla,[2] J. Roque,[3] F. Chalé-Lara,[4] J. K. Olarte,[5] M. Meléndez-Lira,[6] and M. Zapta-Torres[5]

[1]*CONACYT-Centro de Investigación en Ciencia Aplicada y Tecnología Avanzada, Unidad Legaria, IPN, 11500 Ciudad de México, Mexico*
[2]*Facultad de Física, Universidad de La Habana, 10400 La Habana, Cuba*
[3]*Laboratorio Nacional de Nanoscopía Electrónica-CINVESTAV, 07360 Ciudad de México, Mexico*
[4]*Instituto Politécnico Nacional, CICATA Unidad Altamira, C.P, 89600 Altamira, Tamaulipas, Mexico*
[5]*Instituto Politécnico Nacional, CICATA Unidad Legaria, C.P, 11500 Ciudad de México, Mexico*
[6]*Departamento de Física-CINVESTAV, 07360 Ciudad de México, Mexico*

Correspondence should be addressed to N. Cruz-González; nadiacruzgonzalez@gmail.com

Received 9 November 2019; Accepted 5 December 2019; Published 20 January 2020

Guest Editor: Jinliang Li

In the last decade, the urgent need to environmental protection has promoted the development of new materials with potential applications to remediate air and polluted water. In this work, the effect of the TiO_2 thin layer over MoS_2 material in photocatalytic activity is reported. We prepared different heterostructures, using a combination of electrospinning, solvothermal, and spin-coating techniques. The properties of the samples were analyzed by scanning electron microscopy (SEM), transmission electron microscopy (TEM), atomic force microscopy (AFM), X-ray diffraction (XRD), nitrogen adsorption-desorption isotherms, UV-Vis diffuse reflectance spectroscopy (UV-Vis-DRS), and X-ray photoelectron spectroscopy (XPS). The adsorption and photocatalytic activity were evaluated by discoloration of rhodamine B solution. The TiO_2-MoS_2/TiO_2 heterostructure presented three optical absorption edges at 1.3 eV, 2.28 eV, and 3.23 eV. The high adsorption capacity of MoS_2 was eliminated with the addition of TiO_2 thin film. The samples show high photocatalytic activity in the visible-IR light spectrum.

1. Introduction

The growing need to protect the environment promotes the research of heterogeneous photocatalysis as a "green" technique with great potential to remediate air and water pollution. The photocatalysis process, carried out in the presence of a semiconductor, has the ability of removing organic pollutants and heavy metals from wasted water and air, promoting their mineralization into simpler compounds [1, 2]. Titanium dioxide (TiO_2) is the most investigated semiconductor as an oxidizer organic pollutant in water and air, because it is nontoxic and of relatively low cost [3, 4]. The TiO_2 has three crystalline phases anatase, brookite, and rutile; the photocatalytic activity of anatase is always much higher than rutile [5, 6]. The TiO_2 anatase has a large band gap of 3.2 eV, therefore only absorbs ~3-5% of the solar spectrum; this limits its photocatalytic efficiency due to the low electron mobility and high recombination rate of the photogenerated electron-hole pairs [7]. To shift the absorption edge to the visible region and improve the electron-hole separation, the TiO_2 has been modified with different species such as metal and nonmetal ions, rare earth ions, metal

sulfides, and metal oxides [8–14]. The molybdenum disulfide (MoS_2) is a 2D-layered material; in the bulk, the MoS_2 has a band gap of 1.2 eV located on a near-infrared spectrum [15]. When the MoS_2 is exfoliated to give single- or few-layer nanosheets, the optical absorption is blue-shifted with respect to that of the bulk due to quantum confinement effects [16, 17]. The MoS_2 has potential applications in supercapacitors, photocatalytic processes as hydrogen production, or removal of organic pollutants and heavy metals from waste water [18–21]. To obtain the benefits of electronic properties of MoS_2 exfoliated and expand the optical absorption edge of TiO_2 to a solar spectrum, the TiO_2-MoS_2 heterostructures have been synthesized using nanobelts, hollow spheres, and nanofibers using TiO_2 as template by the hydrothermal technique obtaining improvement in the photocatalytic activity and hydrogen production as compared with the use of only TiO_2 or MoS_2 [16, 22, 23]. On the other hand, the MoS_2 has a high adsorption capacity for organic molecules presented in a dye solution [20]. The fast adsorption of molecules from colored solution on the MoS_2 surface happens in the dark phase of adsorption-desorption between photocatalysist and dye solution, previous to light irradiation. However, the organic dye molecules are only adsorbed on the surface of the MoS_2 and have not been degraded, because the catalyst has not been activated yet and the electron-hole pairs has not been generated to carry on the oxidation-reduction reactions. The adsorption of the dyes on MoS_2 could be eliminated if we deposited a layer on this material, which has the characteristics of not adsorbing the dyes. If this material also has the characteristics of being a good photocatalyst (as TiO_2), it would have an important effect on photodegradation. Hočevar et al. reported the preparation of a thin layer of TiO_2 using a Pechini sol-gel method [24]. In the present work, we fabricated a TiO_2-MoS_2/TiO_2 film from MoS_2 nanosheets deposited on TiO_2 nanofibers and covered with a thin layer of TiO_2. We studied the role that plays the thin TiO_2 layer on adsorption and photocatalytic process on the degradation of rhodamine B (RhB) solution under visible-infrared light irradiation.

2. Materials and Methods

The used materials were as follows: PVP (polyvinylpyrrolidone 1,300,000 wt.) from Alfa Aesar; anhydrous ethanol, titanium (IV) isopropoxide 97%, glacial acetic acid, sodium molybdate 98%, thiourea 99% and hydrochloric acid 37%, citric acid 99.5%, and anhydrous ethylene glycol 99.8% from Sigma-Aldrich; and bidistilled water from J.T. Baker.

2.1. Fabrication of TiO_2 Nanofibers. A 13% wt. solution of PVP in anhydrous ethanol was prepared as polymeric solution. The TiO_2 precursor solution was prepared as follows: 1.546 ml of titanium (IV) isopropoxide, 1.905 ml of acetic acid, and 1.270 ml of anhydrous ethanol were mixed and stirred on a magnetic plate for 10 minutes. The TiO_2 precursor solution was added dropwise into polymeric solution and left to stir for 3 h at room temperature for a complete homogenization of the mixture. The TiO_2 polymeric solution was transferred to 5 ml syringe with a stained steel needle of 0.7 mm inner diameter and injected from a syringe pump at 1 ml/h. The distance between needle tip and collector was of 8 cm, and 14 kV was applied to electrospun the polymeric solution. The nanofibers obtained were annealed at 600°C with a heating ramp of 10°C/min, for 5 h under a nitrogen atmosphere to eliminate the organic compounds and crystallize the TiO_2.

2.2. Synthesis of MoS_2 Nanosheets and TiO_2-MoS_2 Heterostructures. The MoS_2 nanosheets were synthetized by a hydrothermal technique as follows: 9.43 g of sodium molybdate and 8.67 g of thiourea were dissolved into 30 ml double distilled water to form a transparent solution and stirred vigorously for 10 min on a magnetic plate, then drops of a 12 M of HCl solution were added until reaching a $pH \leq 1$. The dark blue solution was transferred to a Teflon-lined stainless steel autoclave and heated at 200°C for 24 h. The black precipitate was washed several times with double distilled water, dried at 100°C for 12 h, and grounded until a fine powder was obtained. To synthetize the TiO_2-MoS_2 heterostructures, 0.5 g of annealed TiO_2 nanofibers previously synthetized was added into the MoS_2 precursor solution described above and sonicated for 30 min following the same process.

2.3. Fabrication of TiO_2-MoS_2/TiO_2 Films. The first step in the preparation of the TiO_2-MoS_2/TiO_2 films was the synthesis of a Pechini solution based on a titanium sol. The TiO_2 Pechini solution was prepared from a titanium isopropoxide/citric acid/ethylene glycol solution with a molar ratio of 1 : 4 : 16, respectively. The sol was prepared by mixing of ethylene glycol and titanium isopropoxide into a volumetric flask then heating to 85°C and stirring for 1 h. Finally, citric acid was added and the solution was stirred at this temperature until it turned clear. The second step was the preparation of the mix of TiO_2-MoS_2 powder and the TiO_2 sol as follows: the TiO_2-MoS_2 powder was dissolved into 2 ml of anhydrous ethanol and sonicated for 2 h; then, an amount of TiO_2 sol was added and sonicated for 3 hours; the alcohol in excess was extracted. The molar ratio between the TiO_2-MoS_2 powder and the TiO_2 sol in the mix formulation was 1 : 1. The mix was deposited on a 2.5 cm × 2.5 cm glass substrate, using the spin-coating technique at 1500 rpm for 60 s. Layers were annealed at 450°C for one hour under argon flow. In order to understand the role played by the TiO_2 layer in the adsorption and photocatalytic process, a Pechini solution without the titanium precursor was prepared to deposit the MoS_2 and TiO_2-MoS_2 films without TiO_2 layer. For easy identification, the samples were labeled as follows: MoS_2 without TiO_2 layer (MF), TiO_2-MoS_2 without TiO_2 layer (TMF), MoS_2 with TiO_2 layer (MTF), and TiO_2-MoS_2 with TiO_2 layer (TMTF). Figure 1 shows a scheme of process followed to prepare the heterostructures.

3. Characterization Techniques

The morphology of the heterostructure was studied by a Field Emission-Scanning Electron Microscope (FE-SEM) from (Zeiss, Auriga), operating at 1 kV using the in-lens detector.

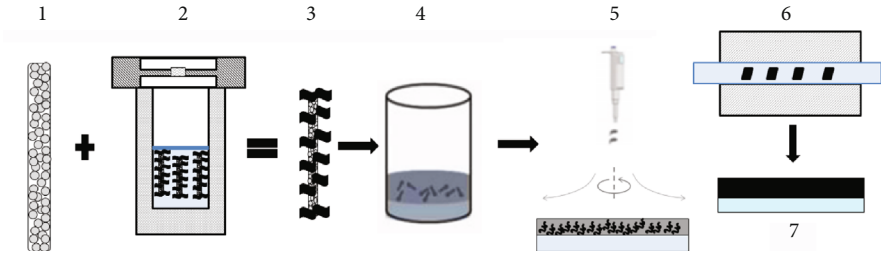

Figure 1: Scheme of process followed to prepare the heterostructures. 1: synthesis of TiO_2 nanofibers by electrospinning, 2: synthesis of TiO_2-MoS_2 by a hydrothermal technique, 3: TiO_2-MoS_2 composite, 4: TiO_2-MoS_2+TiO_2 Pechini solution, 5: spin-coating deposition, 6: thermal annealed, and 7: the TiO_2-MoS_2/TiO_2 heterostructure.

The topography of film was collected from a JSPM-2500 Scanning Probe Microscope of JEOL in tapping mode on the surface of $1.5\,\mu \times 1.5\,\mu$. A high resolution transmission electron microscope (HR-TEM) was carried out with a transmission electron microscope JEOL model JEM-ARM200F operated at 200 kV. The X-ray diffraction (XRD) patterns were collected with an X-ray diffractometer using the CuKα radiation (D8 ECO, Bruker). All samples were analyzed at 40 KV and 40 mA, in the range of 10 to 70° 2-theta degrees with a step size of 0.05° and a step time of 1 s. The diffuse reflectance spectroscopy and the absorption spectra were collected by an Ocean Optics spectrophotometer model USB4000-XR1-ES coupled to UV/Vis/NIR light source model DH-2000. The N_2 adsorption isotherms were carried out with an ASAP 2050 Micrometrics; the samples were activated to 130°C for 6 h; this condition was supplied from the TGA thermogram. In order to understand the effect of the TiO_2 layer over the MoS_2, the TMTF sample, before and after the degradation experiment, was characterized by means of X-ray photoelectron spectroscopy (XPS) (model K alpha by Thermo Scientific). The general survey as well as the high resolution spectra in the regions of the C 1s, O 1s, Ti 2p, S 2p, and Mo 3d was obtained at the surface of the films. The binding energy of the C 1s line at 284.5 eV was taken as the reference peak to calibrate the obtained spectra.

3.1. Photocatalysis Test. The photocatalytic test was performed on discoloration of 80 ml of Rh B solution, with a concentration of 5 mg/l, placed into a 100 ml quartz reactor with a water recirculation system. The irradiation source was provided by a 100 W halogen lamp with a range of 350 nm to 2500 nm (USHIO, USA). The power lamp was modulated by a SORENSEN variable power supply, in order to have wavelengths longer than 400 nm. We found that using a 11.5 V and 7.6 A, the wavelengths were in the range required in the experiment. The samples were vertically placed around the reactor walls and radial irradiated with 87.4 W for 6 h. The residual concentration (C/Co) of Rh B solution was monitored by the variation intensity of the absorption band at 551 nm. Before to the photocatalyst test, the photolysis reaction between the Rh B solution and light source was carried out for 3 h; after that, the dye solution was stirred in the dark for one hour to reach the adsorption-desorption equilibrium. The adsorption-desorption test was performed in the same conditions of the photocatalysis test but in the absence of light for 6 h.

4. Results and Discussion

4.1. Morphological and Crystallinity Structure Analysis. Figure 2(a) shows the SEM image of pure MoS_2; as synthetized, a sphere with a diameter around of 2-3 μm can be observed, with the nanosheets growing perpendicularly to the surface. The image of TiO_2-MoS_2 heterostructures is shown in Figure 2(b); it is observed that a few layers of MoS_2 nanosheets have grown vertically around the TiO_2 nanofibers surface; the diameter of TiO_2 nanofibers was around 250 nm. The superficial TiO_2 grains of the nanofibers form defects that interact with the metallic precursors. In a way, nucleation centers were created that allow the growth of MoS_2 exfoliated nanosheets on the surface of the TiO_2 nanofibers [8]. Figure 2(c) shows the TMTF sample; in the film, the TiO_2-MoS_2 composite was covered with a thin layer of TiO_2; we can observe that film surface has some clusters and cracks produced for the annealing. From the AFM image of Figure 2(d), it is observed that the surface of TMTF is formed for several clusters of material that cause a high roughness. The horizontal and vertical profile graph inside the AFM image confirms the wide height difference between the cluster; also, some cluster separations between them due to the cracks caused by annealing also observed in the SEM image are observed.

Figure 3(a) shows the HRTEM image of the sample TMT; TEM image reveals that the heterostructure was formed for polycrystalline TiO_2 grains and MoS_2 monolayers stacked to form nanosheets deposited onto the TiO_2 surface. From the HAADF image, Figure 3(b), it is observed that the MoS_2 nanosheets were small, their size was around 11 nm wide and 33.2 nm for length, and the distance between monolayers was around 0.69 nm. The FFT (Fast Fourier Transform) inside the HAADF images shows that crystals in the inner of the nanofiber were TiO_2 rutile covered for TiO_2 anatase crystals and the MoS_2 nanosheets formed for around 11 monolayers according to the ICDS cards 202242, 165921, and 24000 for anatase, rutile, and MoS_2-2H molybdenite, respectively.

The XRD patterns of the MTF and TMTF are shown in Figure 3. The XRD pattern of the MTF (Figure 4(a)) exhibits the characteristic diffraction peaks of molybdenite-2H, corresponding to the planes (002), (101), (103), and (110) matched with ICSD-24000. A low intensity TiO_2 diffraction peak at 25.2° was detected; this could be related to the thin layer that coverages the surface of MoS_2 on the film. The

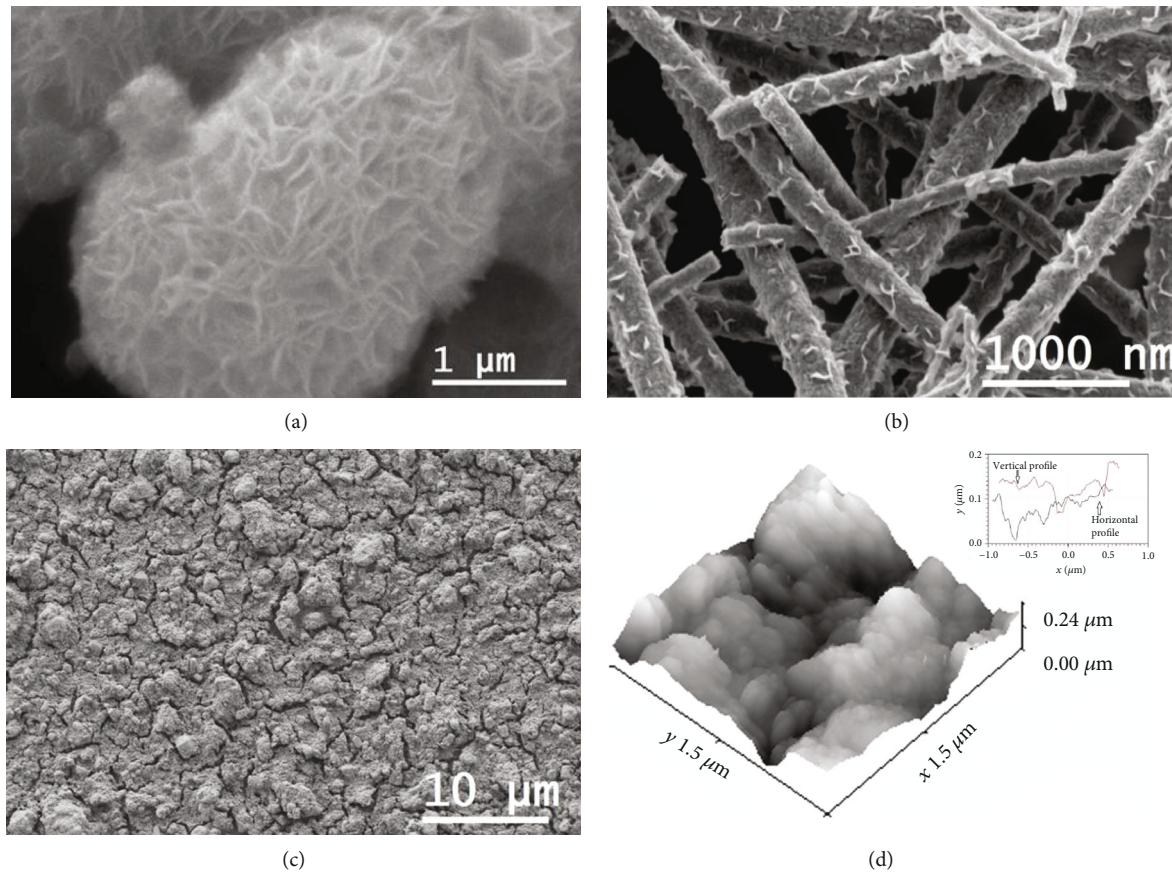

(a) (b) (c) (d)

Figure 2: SEM images of the as-prepared (a) MoS_2, (b) TiO_2-MoS_2 heterostructure, and (c) low magnification of TMTF surface; (d) tapping mode AFM image of TMTF, inside them horizontal and vertical profile graph of surface.

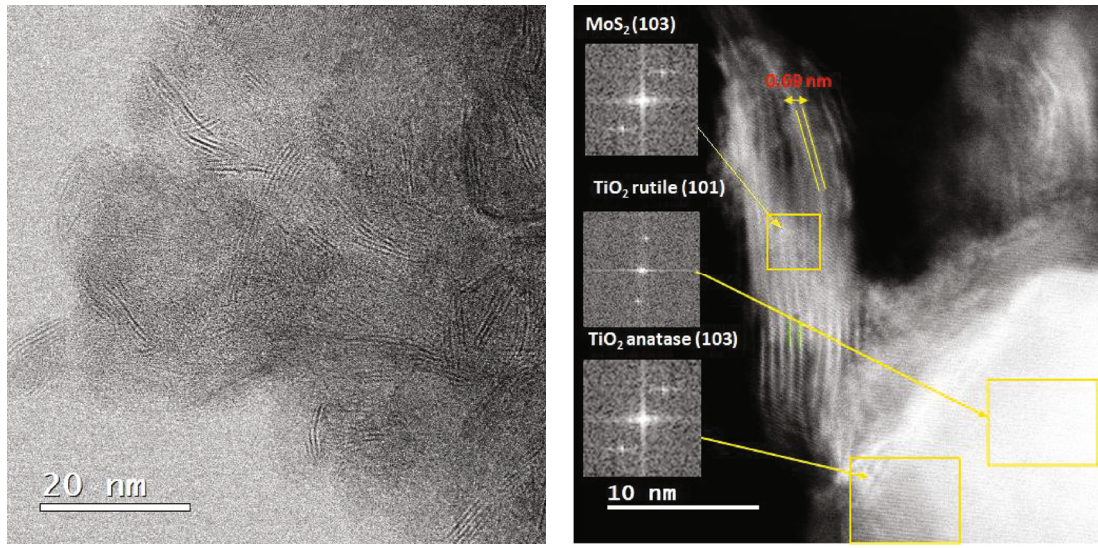

(a) (b)

Figure 3: HR-TEM image of (a) TiO_2-MoS_2 heterostructure and (b) HAADF image for TiO_2-MoS_2 heterostructure, inside FFT images for MoS_2, TiO_2 rutile, and anatase.

diffraction peak at 14.05° corresponds to the "C" axis of the MoS_2; the intensity of this peak is related to the amount of layers stacked in the structure of MoS_2. A monolayer of MoS_2 is composed of Mo atoms coordinated with S atoms to form the S-Mo-S laminated layer [22]. The XRD pattern of the TMTF (Figure 4(b)) shows diffraction peaks assigned

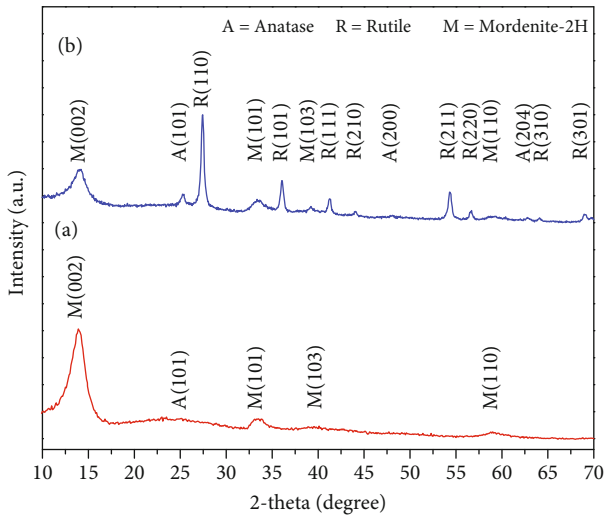

Figure 4: XRD diffractograms of (a) MTF and (c) TMTF after annealed to 450°C.

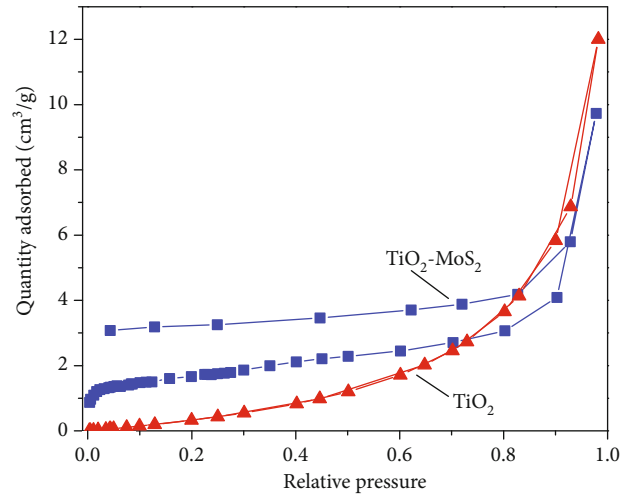

Figure 5: N_2 adsorption isotherms for TiO_2 nanofibers and TiO_2-MoS_2.

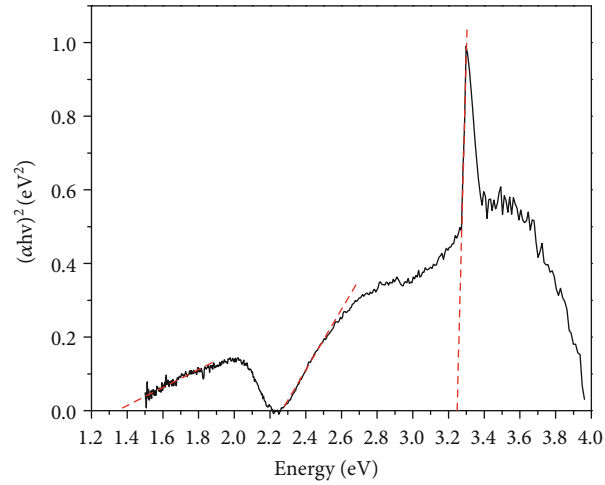

Figure 6: Tauc plot of TMTF sample.

to TiO_2 or MoS_2. The diffraction peaks of MoS_2 have the same position as in the MTF. The diffraction peak at 14.05° is less intense than in the MTF suggesting that the heterostructure is composed for a few monolayers of MoS_2 [25], which are what give rise to the nanosheets according to observations in Figure 2(a). Most of TiO_2 diffraction peaks were matched to rutile phase corresponding to the planes (110), (101), (111), (210), (211), (220), (310), and (301) according to ICSD-165921. The presence of rutile is due to the influence of gas used in the annealing of TiO_2 nanofibers as observed in previous work [26]. Few weak anatase diffraction peaks were observed corresponding to the planes (101), (200), and (204) according to the ICSD-202242. The anatase reflection is from the TiO_2 thin layer that coverages the surface of the heterostructure.

The nitrogen adsorption-desorption isotherms of the TiO_2 nanofibers and TiO_2-MoS_2 heterostructures, Figure 5, were used to estimate the BET surface area. The TiO_2 nanofibers show a greater specific surface area (19.9 m^2/g) than that of TiO_2-MoS_2 heterostructure; when the MoS_2 nanosheets grew up on the TiO_2 nanofiber surface, the specific surface area reduces to 7.87 m^2/g because the pores in TiO_2 nanofibers were occupied with MoS_2 nanosheets. Additionally, both materials are mesoporous structure; this result is consistent with that reported by Liu et al. [16].

4.2. Optical Properties. The band gap energy (E_g) values of TMTF were determined through diffuse reflectance spectroscopy, plotting the $[\alpha(h\nu)h]^2$ vs. photon energy ($h\nu$) axis and extrapolating the linear portion of the absorption edge to zero [27]. Figure 6 shows the Tauc plot for the TMTF is possible to note three optical adsorption edges at 1.3 eV, 2.28 eV, and 3.23 eV. The first one (1.3 eV) is due to the presence of MoS_2 bulk. The second one (2.25 eV) maybe related to quantum confinement due to nanosheet exfoliation as observed in the TEM image; Quinn et al. obtained MoS_2-exfoliated monolayers with a band gap of 1.97 eV [28]; it can also be related to the formation of electronic traps between the heterostructure junctions. The last one (3.23 eV) corresponds to the TiO_2 anatase layer that coverages the surface of film.

4.2.1. X-Ray Photoelectron Spectroscopy. In order to investigate the formation and the stability of the external layer of TiO_2, the sample TMTF was characterized before and after the degradation experiment. The chemical composition and chemical state were identified with the help of XPS analysis; the binding energy of the peaks were obtained from XPS database of NIST [29]. The XPS spectra of the TMTF sample: (a) survey, (b) Ti 2p, (c) S 2p, and (d) Mo 3d, are shown in Figures 7(a)–7(d). From Figure 7(a), the elements S, Mo, C, Ti, and O are observed in the XPS survey spectrum, which confirms the formation of the superficial TiO_2 layer; the presence of Mo and S elements is related to the MoS_2 intermediate layer, and the thickness of the TiO_2 overlayer is less than 10 nm. In Figure 7(b), the high resolution spectra of Ti 2p is presented; a doublet is observed with one peak related to Ti $2p_{3/2}$ and the other to Ti $2p_{1/2}$ with binding energies of

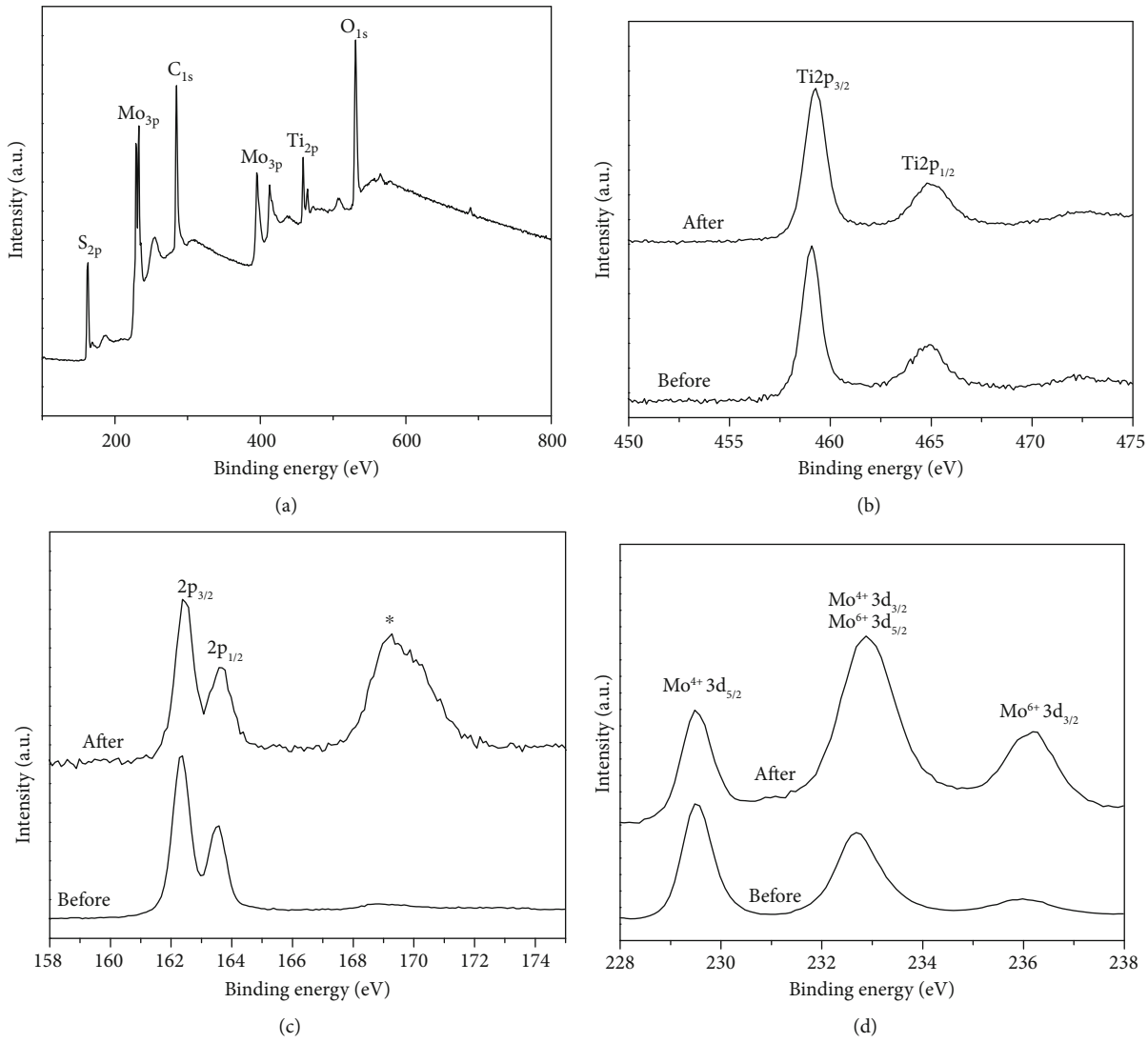

Figure 7: XPS spectra of TMTF sample (a) general survey, (b) high resolution of Ti 2p, (c) high resolution of S 2p, and (d) high resolution Mo 3d. The label before and after means before and after photocatalytic experiment.

459.0 eV and 464.7 eV, respectively. The binding energies found are related to the Ti with the chemical environment of TiO_2. It can be observed that the peaks presented stability after the degradation experiment, suggesting that our external layer is stable. The high resolution spectra of the S 2p is presented in Figure 7(c); the presence of a doublet related to S $2p_{3/2}$ and S $2p_{1/2}$ at binding energies of 162.3 eV and 163.6 eV, respectively, can be seen. After the photodegradation experiment, additional peak appears at a binding energy of 169 eV (labeled in the figure with *); the presence of this peak had been reported previously [30, 31] in TiO_2 doped with S; this peak disappears after the sample was eroded with argon ions. The presence of this peak could be related to the fact that we deposited a thin layer of precursor solution of TiO_2 over MoS_2; then, a thermal annealing was applied at the sample and a sulfur diffusion on TiO_2 was promoted. Hence, the peak could be due to the binding of sulfur with the adsorbed dye in the surface of the sample, and when we eroded with argon ions, we eliminated the adsorbed dye and the peak disappears. The high resolution spectrum of Mo 3d (Figure 7(d)) can be separated into two doublets. The first doublet at 229.6 eV and 232.7 eV is related to Mo $3d_{5/2}$ and Mo $3d_{3/2}$, related to Mo^{4+} of the MoS_2 compound; the second at 233.4 eV and 236.5 eV is related to Mo $3d_{5/2}$ and Mo $3d_{3/2}$, related to Mo^{6+} of the MoO_3 compound. Similar results had been reported by Senthil et al. [32].

4.3. Photocatalytic Activity. The aim of this work is to evaluate the effect of the TiO_2 thin layer over the MoS_2; then, it has been evaluated on the adsorption-desorption capacity and their photocatalysis activity on the degradation of Rh B solution in the dark and Vis-IR light, respectively. Figure 8 shows the variation of residual concentration (C/Co) with the time of the Rh B solution in the dark in the presence of the films. The films without a TiO_2 thin layer coating in the surface of heterostructure, MF and TMF, show that the adsorption-desorption equilibrium between the photocatalyst and the dye solution is not reached after 6 h. The constant

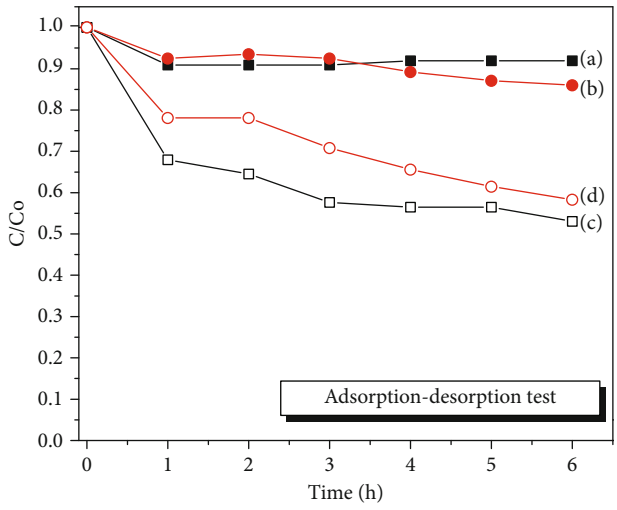

(a) MTF
(b) TMTF
(c) MF
(d) TMF

Figure 8: Adsorption-desorption test between Rh B solution in the presence of different photocatalyst. The test was carried out in the dark.

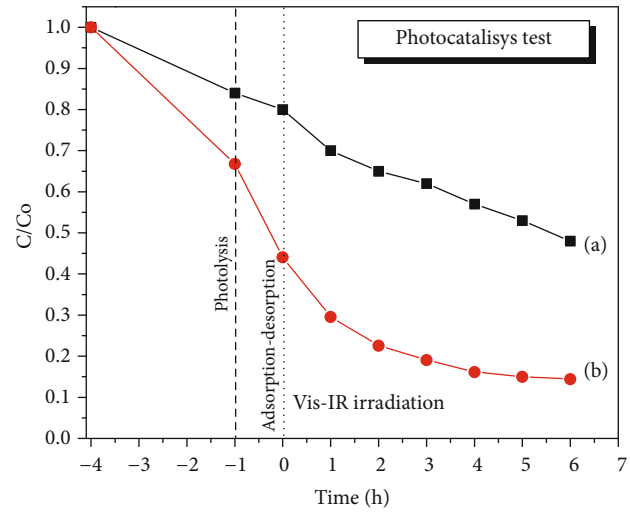

(a) MTF
(b) TMTF

Figure 9: Photocatalytic test between Rh B solution in the presence of different photocatalyst. The test was carried out under Vis-IR light.

discoloration in the dark of the dye solution is due to the MoS_2 as 2D-layered nanomaterials that had excellent anchoring surface for adsorbing dye molecules [33]. But the Rh B molecules are being superficially adsorbed on MoS_2, and not necessarily degraded. After 6 h of contact, about 50% of solution was discolored for both samples. Instead with the films coating with a TiO_2 thin layer, MTF and TMTF were placed in contact to dye solution in the dark; the adsorption-desorption equilibrium was reached in the first hour, and the concentration of Rhodamine B solution remained constant after 6 h. The obtained result indicates that the TiO_2 thin layer coating the heterostructure decreases drastically the adsorption capacity of MoS_2. Now, the adsorption of organic molecules is carried out on the TiO_2 surface.

Figure 9 shows the photocatalysis degradation of Rh B solution in the presence MTF and TMTF under Vis-IR light irradiation. The variation of residual concentration (C/Co) with the time is observed. The TMTF shows a better photocatalytic activity; it is related to the band gap energy; the TMTF shows an absorption edge in the visible and near-infrared; then, the catalyst is photoactive in a larger region of the solar spectrum. Additionally, the high roughness of TMTF as observed in AFM images provides more contact surface to interact with the dye solution. After 6 h of irradiation, the 90% of Rh B solution was degraded for the TMTF. Taking into account that the discoloration of Rh B solution produced by the photolysis and adsorption effect were made before the irradiation, all discoloration of dye during the photocatalysis test is due to oxidation-reduction reaction between photocatalyst and organic molecules from dye solution.

Liu et al. [7] determined the band alignment for the TiO_2/multilayer MoS_2 interfaces; they report the valence band offset (VBO) and conduction band offset (CBO) of TiO_2/ML-MoS_2 interfaces were 2.28 eV and 0.28 eV, respectively. A possible process for photogeneration electron-hole pairs and the transfers between TiO_2 and MoS_2 into the heterostructure is described below, a schematic illustration is shown in Figure 10.

(1) The photons from the Vis-IR light are absorbed by the MoS_2, generating the electron-hole pairs

(2) When the energy of electrons in CBO is bigger than 0.28 between MoS_2 and TiO_2, the electron in the conduction band (CB) of MoS_2 is transmitted to the CB of the TiO_2

(3) An electron from the CB of TiO_2 is displaced and reacts with oxygen to produce superoxide anion radicals

(4) Simultaneously, the electrons from the valence band (VB) of TiO_2 absorb the energy needed to overcome the VBO between TiO_2 and MoS_2 and compensate the electronic vacancy in the VB of MoS_2

(5) The hole generated in the VB of TiO_2 reacts with rhodamine B and is degraded

A possible mechanism for RhB degradation by the TiO_2-MoS_2/TiO_2 composites includes the possible steps listed below. The enhanced photocatalytic performance of the TiO_2-MoS_2/TiO_2 composites could result from the charge transfer process between MoS_2 and TiO_2. Under Vis-IR light irradiation, electrons and hole pairs were produced on MoS_2 of CB and VB, respectively (equation (1)). When the MoS_2 electrons have an energy bigger than the CBO, the electron in the conduction band (CB) of MoS_2 is transmitted to the CB of the TiO_2 (equation (2)). The electrons on the conduction band of TiO_2 react with adsorbed O_2 on the surface of the photocatalysts and produce superoxide radical ($\dot{O}_2^-$) to

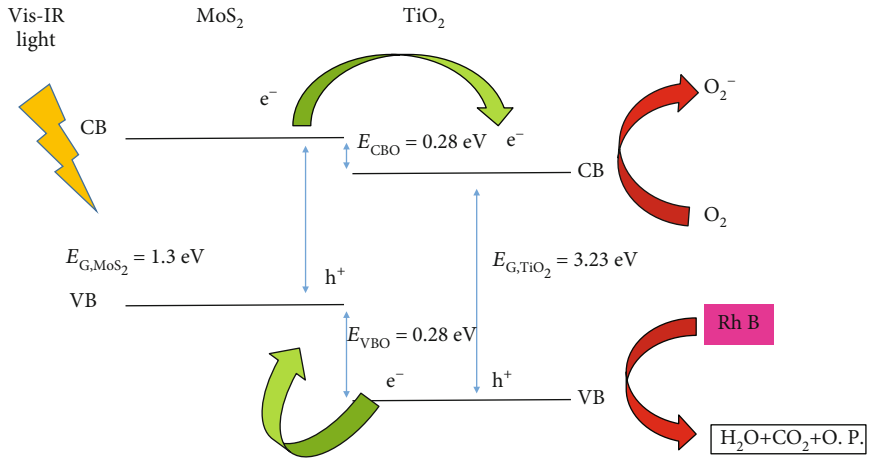

Figure 10: Schematic illustration of charge transfer of TiO_2-MoS_2/TiO_2 film in the visible-infrared light.

oxidize RhB (equation (3)). On the other hand, when the electrons from the valence band (VB) of TiO_2 absorb the energy needed to overcome the VBO between TiO_2 and MoS_2 and compensate the electronic vacancy in the VB of MoS_2 and generated a hole (h^+) in the VB of TiO_2 (equation (4)), the (h^+) generated in the VB of TiO_2 reacts with the rhodamine B producing an oxidized $RhB^{+\cdot}$ that in the presence of O_2 dissolved in water is reduced to rhodamine as intermediate (equations (5) and (6)); other (h^+) from VB of TiO_2 dissociates the H_2O in $OH^{\cdot}$ and H^+ (equation (7)); simultaneously, the RhB reaction with the $^{\cdot}O_2$- or $^{\cdot}OH$ or H^+ generated from other reactions to finally produce carbon dioxide and water (equations (8) and (9)).

$$MoS_2 + hv_{(Vis-IR)} \longrightarrow MoS_2(e^-) + MoS_2(h^+) \quad (1)$$

$$MoS_2(e^-) + TiO_2 \longrightarrow MoS_2 + TiO_2(e^-) \quad (2)$$

$$TiO_2(e^-) + O_2 \longrightarrow O_2^{-\cdot} + TiO_2 \quad (3)$$

$$2TiO_2 + hv_{(VBO)} + MoS_2(h^+) \longrightarrow MoS_2 + TiO_2(h^+) \quad (4)$$

$$TiO_2(h^+) + RhB \longrightarrow RhB^{+\cdot} + TiO_2 \quad (5)$$

$$RhB^{+\cdot} + O_2 \longrightarrow Rhodamine \quad (6)$$

$$H_2O + TiO_2(h^+) \longrightarrow OH^{\cdot} + H^+ + TiO_2 \quad (7)$$

$$RhB + O_2^{\cdot -}/{}^{\cdot}OH \longrightarrow Products \quad (8)$$

$$RhB + H^+ \longrightarrow CO_2 + H_2O + other\ products \quad (9)$$

5. Conclusions

The thin layer of TiO_2 that coverages the MoS_2 and TiO_2-MoS_2 to form the heterostructure film practically eliminate the strong adsorption capabilities of the MoS_2 in the dark. The heterostructures show excellent photocatalytic activities under visible to infrared light illumination. The photocatalysis activity was superior to MoS_2/TiO_2 film. The heterostructures might have promising applications in polluted water treatment and facile recovery to reuse.

Data Availability

The XRD, DRS, and SEM, XPS, AFM, TEM images and absorbance spectra data used to support the findings of this study are available from the corresponding author upon request.

Conflicts of Interest

The authors declare that there is no conflict of interests regarding the publication of this paper.

Acknowledgments

The authors want to acknowledge to the Research and Postgraduate Secretary of Instituto Politécnico Nacional for the financial support by the project SIP-IPN (20190155).

References

[1] X. Liu, B. Liu, L. Li et al., "$Cu_2In_2ZnS_5$/Gd_2O_2S:Tb for full solar spectrum photoreduction of Cr(VI) and CO_2 from UV/vis to near-infrared light," *Applied Catalysis B: Environmental*, vol. 249, pp. 82–90, 2019.

[2] B. Liu, X. Liu, J. Liu et al., "Efficient charge separation between UiO-66 and $ZnIn_2S_4$ flowerlike 3D microspheres for photoelectronchemical properties," *Applied Catalysis B: Environmental*, vol. 226, pp. 234–241, 2018.

[3] C. B. Almquist and P. Biswas, "Role of synthesis method and particle size of nanostructured TiO_2 on its photoactivity," *Journal of Catalysis*, vol. 212, no. 2, pp. 145–156, 2002.

[4] M. Andersson, L. Österlund, S. Ljungström, and A. Palmqvist, "Preparation of nanosize anatase and rutile TiO_2 by hydrothermal treatment of microemulsions and their activity for photocatalytic wet oxidation of phenol," *The Journal of Physical Chemistry. B*, vol. 106, no. 41, pp. 10674–10679, 2002.

[5] A. Sclafani and J. M. Herrmann, "Comparison of the photoelectronic and photocatalytic activities of various anatase and rutile forms of titania in pure liquid organic phases and in

aqueous solutions," *The Journal of Physical Chemistry*, vol. 100, no. 32, pp. 13655–13661, 1996.

[6] J. Li, X. Xu, X. Liu, W. Qin, M. Wang, and L. Pan, "Metal-organic frameworks derived cake-like anatase/rutile mixed phase TiO_2 for highly efficient photocatalysis," *Journal of Alloys and Compounds*, vol. 690, pp. 640–646, 2017.

[7] X. Liu, L. Chen, Q. Liu et al., "Band alignment of atomic layer deposited TiO_2/multilayer MoS_2 interface determined by _x_ -ray photoelectron spectroscopy," *Journal of Alloys and Compounds*, vol. 698, pp. 141–146, 2017.

[8] Z. Zhang, C. Shao, L. Zhang, X. Li, and Y. Liu, "Electrospun nanofibers of V-doped TiO_2 with high photocatalytic activity," *Journal of Colloid and Interface Science*, vol. 351, no. 1, pp. 57–62, 2010.

[9] J. Xu, Y. Ao, D. Fu, and C. Yuan, "A simple route for the preparation of Eu, N-codoped TiO_2 nanoparticles with enhanced visible light-induced photocatalytic activity," *Journal of Colloid and Interface Science*, vol. 328, no. 2, pp. 447–451, 2008.

[10] Y. Yang, C. Zhang, Y. Xu, H. Wang, X. Li, and C. Wang, "Electrospun Er:TiO_2 nanofibrous films as efficient photocatalysts under solar simulated light," *Materials Letters*, vol. 64, no. 2, pp. 147–150, 2010.

[11] N. Qin, Y. Liu, W. Wu et al., "One-dimensional CdS/TiO2Nanofiber composites as efficient visible-light-driven photocatalysts for selective organic transformation: synthesis, characterization, and performance," *Langmuir*, vol. 31, no. 3, pp. 1203–1209, 2015.

[12] Z. Chen, J. Zhao, X. Yang et al., "Fabrication of TiO_2/WO_3 composite nanofibers by electrospinning and photocatalystic performance of the resultant fabrics," *Industrial and Engineering Chemistry Research*, vol. 55, no. 1, pp. 80–85, 2016.

[13] J. Li, X. Xu, X. Liu et al., "Sn doped TiO_2 nanotube with oxygen vacancy for highly efficient visible light photocatalysis," *Journal of Alloys and Compounds*, vol. 679, pp. 454–462, 2016.

[14] J. Li, X. Xu, X. Liu, W. Qin, and L. Pan, "Novel cake-like N-doped anatase/rutile mixed phase TiO_2 derived from metal-organic frameworks for visible light photocatalysis," *Ceramics International*, vol. 43, no. 1, pp. 835–840, 2017.

[15] S.-M. Paek, H. Jung, M. Park, J. K. Lee, and J. H. Choy, "An inorganic nanohybrid with high specific surface area: TiO_2-pillared MoS_2," *Chemistry of Materials*, vol. 17, no. 13, pp. 3492–3498, 2005.

[16] C. Liu, L. Wang, Y. Tang et al., "Vertical single or few-layer MoS_2 nanosheets rooting into TiO_2 nanofibers for highly efficient photocatalytic hydrogen evolution," *Applied Catalysis B: Environmental*, vol. 164, pp. 1–9, 2015.

[17] T. Li and G. Galli, "Electronic properties of MoS_2 nanoparticles," *Journal of Physical Chemistry C*, vol. 111, no. 44, pp. 16192–16196, 2007.

[18] K. J. Huang, L. Wang, Y. J. Liu et al., "Layered MoS_2-graphene composites for supercapacitor applications with enhanced capacitive performance," *International Journal of Hydrogen Energy*, vol. 38, no. 32, pp. 14027–14034, 2013.

[19] J. C. Tokash and B. E. Logan, "Electrochemical evaluation of molybdenum disulfide as a catalyst for hydrogen evolution in microbial electrolysis cells," *International Journal of Hydrogen Energy*, vol. 36, no. 16, pp. 9439–9445, 2011.

[20] X. Bai, J. Wan, J. Jia et al., "Simultaneous photocatalytic removal of Cr(VI) and RhB over 2D MoS_2/red phosphorus heterostructure under visible light irradiation," *Materials Letters*, vol. 222, pp. 187–191, 2018.

[21] Z. Ren, X. Liu, Z. Zhuge, Y. Gong, and C. Q. Sun, "$MoSe_2$/ZnO/ZnSe hybrids for efficient Cr(VI) reduction under visible light irradiation," *Chinese Journal of Catalysis*, vol. 41, no. 1, pp. 180–187, 2020.

[22] W. Zhou, Z. Yin, Y. du et al., "Synthesis of few-layer MoS2 nanosheet-coated TiO_2 nanobelt heterostructures for enhanced photocatalytic activities," *Small*, vol. 9, no. 1, pp. 140–147, 2013.

[23] J. Wang, B. Wei, L. Xu, H. Gao, W. Sun, and J. Che, "Multilayered MoS_2 coated TiO_2 hollow spheres for efficient photodegradation of phenol under visible light irradiation," *Materials Letters*, vol. 179, pp. 42–46, 2016.

[24] M. Hočevar, U. O. Krašovec, M. Berginc, and M. Topič, "One step preparation of TiO_2 layer for high efficiency dye-sensitized solar cell," *Acta Chimica Slovenica*, vol. 57, no. 2, pp. 405–409, 2010.

[25] K. Chang and W. Chen, "Single-layer MoS2/graphene dispersed in amorphous carbon: towards high electrochemical performances in rechargeable lithium ion batteries," *Journal of Materials Chemistry*, vol. 21, no. 43, pp. 17175–17184, 2011.

[26] N. Cruz-González, J. L. Fernández Muñoz, M. Zapata-Torres, and M. García-Hipólito, "Efecto del gas utilizado en el tratamiento térmico y la impurificación con Eu en las propiedades estructurales de nanofibras de TiO_2 depositadas por electrohilado," *Superficies y vacío*, vol. 26, no. 3, pp. 111–116, 2013.

[27] M. Nowak, B. Kauch, and P. Szperlich, "Determination of energy band gap of nanocrystalline SbSI using diffuse reflectance spectroscopy," *Review of Scientific Instruments*, vol. 80, no. 4, p. 046107, 2009.

[28] M. D. J. Quinn, N. H. Ho, and S. M. Notley, "Aqueous dispersions of exfoliated molybdenum disulfide for use in visible-light photocatalysis," *ACS Applied Materials & Interfaces*, vol. 5, no. 23, pp. 12751–12756, 2013.

[29] http://srdata.nist.gov/XPS/.

[30] X. Yang, C. Cao, L. Erickson, K. Hohn, R. Maghirang, and K. Klabunde, "Photo-catalytic degradation of rhodamine B on C-, S-, N-, and Fe-doped TiO_2 under visible-light irradiation," *Applied Catalysis B: Environmental*, vol. 91, no. 3–4, pp. 657–662, 2009.

[31] S. A. Bakar and C. Ribeiro, "Prospective aspects of preferential {001} facets of N,S-co-doped TiO_2 photocatalysts for visible-light-responsive photocatalytic activity," *RSC Advances*, vol. 6, no. 92, pp. 89274–89287, 2016.

[32] R. A. Senthil, S. Osman, J. Pan, Y. Sun, T. R. Kumar, and A. Manikandan, "A facile hydrothermal synthesis of visible-light responsive $BiFeWO_6$/MoS_2 composite as superior photocatalyst for degradation of organic pollutants," *Ceramics International*, vol. 45, no. 15, pp. 18683–18690, 2019.

[33] T. F. Jaramillo, K. P. Jorgensen, J. Bonde, J. H. Nielsen, S. Horch, and I. Chorkendorff, "Identification of active edge sites for electrochemical H_2 evolution from MoS_2 nanocatalysts," *Science*, vol. 317, no. 5834, pp. 100–102, 2007.